Intelligent Positioning Enhancement Methodology for Tightly Coupled GNSS/INS in Different Occluded Environments

BaiDan LI[1]*, GuoXing RUAN[1], MinCong TANG[2], WenXi YANG[1]

[1] Transport Planning and Research Institute Ministry of Transport, Building 2, No.6 Shuguang Xili Jia, Chaoyang District, Beijing, 100029, China
115272572@qq.com (**Corresponding author*), 526434753@qq.com, yangwx_yang@163.com

[2] Industrial University of Ho Chi Minh City, Ho Chi Minh, Vietnam
mincongtang@iuh.edu.cn

Abstract: This paper proposes an intelligent positioning enhancement methodology on the basis of tightly coupled GNSS-INS integration. The basic idea of this paper is to make full use of the visible satellite observations for measurement update in occluded environments, and then execute the positioning enhancement based on intelligent models. According to the position error characteristics for a varying number of visible satellites in different occluded environments, different positioning enhancement strategies are adopted. For the case involving two or three visible satellites, a joint estimation model for satellite position and pseudo-range based on multi-task learning is designed in order to supplement the satellite observations, and thereby satisfying 4 satellites to achieve accurate localization solving. For the case involving zero visible satellites or one visible satellite, a hybrid temporal neural network, which is compatible with INS and/or satellite inputs, is designed for localization error prediction and compensation. With the purpose of verifying the feasibility and effectiveness of the proposed methodology, road-test experiments with various driving scenarios were performed. The experimental results demonstrate the superiority of the proposed methodology over all the other employed methods.

Keywords: Vehicle Positioning, Intelligent Enhancement, Tightly Coupled, Multi-task Learning, Input Compatibility.

1. Introduction

An accurate and reliable positioning are very important for advanced vehicular applications and Intelligent Transportation Systems (ITSs). Due to the complementary characteristics of the Global Navigation Satellite System (GNSS) and Inertial Navigation System (INS), the GNSS/INS integrated system is the most widespread technology used in vehicle localization (Adusumilli et al., 2015; Murugaiah, Samiappan & Nagu, 2025). When GNSS is available, it can provide accurate absolute position and velocity information. When GNSS fails, the INS is not affected by external disturbances and can bridge GNSS (Ando et al., 2021).

However, due to the frequent GNSS signal occlusion caused by overpasses, skyscrapers, tunnels, etc. in urban environments, the positioning system is still prone to large cumulative errors when relying only on INS (Bai et al., 2020). Achieving a high-reliability positioning in urban environments is still a major challenge.

One of the popular strategies consists in introducing external observation by adding additional sensors such as cameras, radar, and Lidar (Chu et al., 2021; Wang, Liang & Zhao, 2025). The complementary characteristics of different sensors can improve the adaptivity of the positioning systems in complex urban environments. However, additional sensors will require a more complex calibration and synchronization, while also introducing an extra cost to a certain extent..

With the development of artificial intelligence (AI) and big data, AI-related solutions are explored so as to improve the positioning accuracy during GNSS outages. The error prediction and compensation solutions based on AI can be classified into two categories:

1. Predicting the INS position error - The aim is to establish the model of the INS error, the related input includes the time, INS noise, vehicle motion etc. Then, the final positioning results can be compensated by the predicted INS error;

2. Predicting the GNSS-related information - The mapping relationship between the GNSS position increment in adjacent moments and vehicle motion is established. The pseudo-GNSS position observation can be obtained by accumulating GNSS position increment and it is fused with the INS position to obtain the final position output. Besides, certain research works also use the GNSS position and pseudo-range prediction to enhance the performance of the GNSS/INS integrated system.

https://doi.org/10.24846/v35i2y202610

It should be noted that the two above-mentioned categories of methods are applied in a loosely coupled mode, i.e. only the two states of GNSS validity and failure are considered, and the measurement update for visible satellite observations is not taken into consideration. In fact, even if there are less than 4 visible satellites to complete the high-precision position calculation, the GNSS does not completely fail in most cases, the observations of visible satellites are still available in occluded environments (Farag, 2021). The information provided by the visible satellites can still be involved in the measurement update during fusion positioning.

The loosely coupled integrated positioning system uses GNSS positions as observations. When the number of satellites received by the receiver is lower than 4, the GNSS is unable to provide position information, and thus the fusion positioning algorithm is unable to execute a measurement update properly. On the other hand, the tightly coupled GNSS/INS integrated positioning system uses pseudo-range prediction or the pseudo-range rate as observations (Gao et al., 2022). When the number of visible satellites is lower than 4, the fusion positioning algorithm can still utilize partial observations of the visible satellites to carry out the measurement update and correct the INS errors.

For a set of GNSS and INS data collected in an open field, where the GNSS can receive a sufficient number of visible satellites, a varying number of satellites is selected artificially for tightly coupled fusion positioning. It can be found that, for 0 satellites or 1 selected satellite, the INS error dominates, and the localization error is cumulative. For 2 or 3 selected satellites, the correction of the visible satellite observation is obvious, and the localization error is significantly reduced compared with the case involving 0 and 1 visible satellite. Besides, the localization error does not become cumulative over time. However, compared with the case of fusing 4 or more satellites, the positioning error is still large. For the case involving 4 selected satellites, the positioning accuracy is close to that obtained for the case involving all satellites. Thus, in most cases, good localization results can be achieved with 4 satellites.

Based on the above analysis, the localization error characteristics for 0 or 1 satellite and for 2 or 3 satellites are entirely different. So, the GNSS occluded environment can be characterised as mildly occluded with 2 or 3 received satellites and severely occluded with 0 satellites or 1 received satellite. Then, different positioning error correction strategies are adopted. For the mildly occluded environment, a multi-task learning-based GNSS observation enhancement model is constructed to predict the satellite position and pseudo-range of the failed satellites, so as to make up the GNSS observation to 4 satellites. For the severely occluded environment, a localization error prediction model based on a hybrid temporal neural network is implemented, which is compatible with the different input for the scenario involving 0 satellites or 1 visible satellite, and then the predicted localization error is used for compensation. The novel aspects presented in this paper can be summarized as follows:

1. An intelligent positioning enhancement methodology is proposed for GNSS/INS in the tightly coupled mode, which can make full use of the visible satellite observations. According to the error characteristics of tightly coupled positioning with a varying number of satellites, different error compensation (positioning enhancement) strategies are adopted;

2. For the case involving 2 or 3 visible satellites, the position errors show weak time-accumulation characteristics, and a joint estimation model for satellite position and pseudo-range based on multi-task learning is designed to improve the positioning accuracy from the perspective of supplementing satellite observations. For the case involving 0 satellites or 1 visible satellite, the position errors feature obvious time-accumulation characteristics, and a hybrid temporal neural network is designed for position error prediction and compensation, which is compatible with different INS and satellite inputs.

The remainder of this paper is organized as follows. Section 2 reviews the related studies on GNSS/INS positioning enhancement, including INS position error prediction and GNSS-related information prediction methods. Section 3 presents the overall framework of the proposed intelligent positioning enhancement methodology for different occluded environments. Further on, Section 4 details the GNSS observation enhancement model based on multi-task learning for mildly occluded environments with two or three visible satellites. Section 5 describes the localization error prediction model based on a hybrid temporal neural network for severely occluded environments with zero visible

satellites or one visible satellite. Section 6 reports the experimental validation and analyzes the positioning performance of the proposed method under different satellite visibility conditions. Finally, Section 7 concludes the paper and outlines future research directions.

2. Related Works

The AI-based models for bridging GNSS outages for GNSS/INS integrated systems have attracted much attention in recent years, leading to the emergence of many works. The main idea of these solutions is to provide some support information for GNSS or INS. When GNSS works well, an AI module is trained, which is constructed to explore the relationship between the vehicle`s dynamics and the demanded support information. When GNSS signals are weak or missing, the well-trained AI module will predict the demanding information, such as the GNSS position increment, satellite pseudo-range, and INS position errors. According to different outputs, these AI-based models are mainly divided into the following two categories.

2.1 Predicting INS Position Error

Li et al. (2017) employed the ensemble learning algorithm to model the INS position error based on current samples and some past samples of INS velocity, attitude, acceleration, and angular velocity. Adusumilli et al. (2015) claimed that in order to address the issues of poor generalization capability and overfitting caused by the noise, the INS position error was modeled by a hybrid method involving Principal Component Regression and Random Forest Regression.

Besides, Li & Xu (2017) have also been carried out in this area. On the basis of in-vehicle sensor assistance, a grey model-based scheme was proposed that used only historical INS errors for prediction (Li & Xu, 2017), as well as a hybrid predictor comprising an online-trained Autoregressive Integrated Moving Average model and an offline-trained Extreme Learning Machine model which elaborately considered the INS noise characteristics.

2.2 Predicting GNSS-related Information

GNSS-related information mainly refers to the GNSS position increment, and the GNSS position and satellite pseudo-range are also included.

Liu & Guo (2021) proposed a multiple long short-term memory (multi-LSTM) module to predict the increment of the GNSS position, and an improved extended Kalman filter was maintained to obtain the position during GNSS outages. Liu et al. (2022) combined a convolutional neural network and a gated recurrent unit neural network to model the relationship among the attitude, specific force, angular rate, and the GNSS position increment. Fang et al. (2020) employed the LSTM algorithm to construct a relationship between the present and past information to generate the pseudo-GNSS position increment. Yao et al. (2017) established an improved Multi-Layer Perceptron network to directly relate the velocity, angular rate, and specific force of INS to the GNSS position increment, thereby providing pseudo position information to assist the GNSS/INS integrated navigation system.

Besides, Lu et al. (2020) proposed a heterogeneous multi-task learning structure with a shared de-noising process to conduct pseudo-GPS position prediction. Sun et al. (2021) stated that the pseudo-range errors were predicted by means of an ensemble bagged regression tree model accounting for signal strength, satellite elevation angle, and coordinate information. Liu, Luo & Zhou (2022) constructed a non-line-of-sight (NLOS) signal detection model based on a convolutional neural network and the detected NLOS signals were decomposed using the variational mode decomposition method to eliminate the NLOS part and improve the data quality.

The feasibility of all the above-mentioned methods has been validated in simulations, real field tests, or through public data tests.

In conclusion, the existing position error compensation methods discard the observations of partially visible satellites. This paper focuses on improving the performance of GNSS/INS integration based on the utilization of the available observations of the visible satellites in occluded environments.

3. Overview of The Proposed Methodology

By analyzing the influence of a varying number of satellites on the positioning results, this paper further subdivided the occluded environments into mildly occluded environments (the number of visible satellites is 3 or 2) and severely occluded

environments (the number of visible satellites is 1 or 0). Consequently, two distinct positioning enhancement methods are proposed for the two kinds of occluded environments, effectively utilizing the partial satellite signals that can still be received in occluded environments.

For the mildly occluded environment, a satellite position and pseudo-range joint prediction network based on multi-task learning is designed, and a tightly coupled fusion localization method based on GNSS observation enhancement is implemented to obtain the vehicle position, as shown in Figure 1.

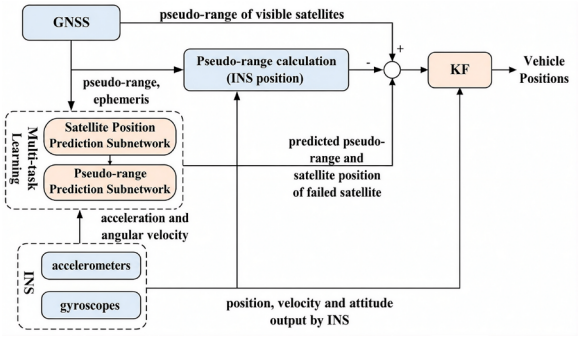

Figure 1. Diagram of the proposed positioning methodology (for the mildly occluded environment)

When the vehicle is driving in a mildly occluded environment, the received satellite signals and INS output at previous moments are taken as the inputs of a multi-task learning model, and the positions and pseudo-ranges of the failed satellite are predicted at the same time. Although it is possible to calculate the satellite positions with previously received ephemeris data, this method has errors in solving the positions of failed satellites with regard to localizing the failed satellites. Considering the correlation between satellite positions and pseudo-ranges, a joint multi-task estimation is performed. The multi-task loss balance method based on training speed is used for optimizing the model.

Finally, the satellite position and pseudo-range predicted by the multi-task learning model, the available satellite observations received by the GNSS receiver, as well as the INS information are fused based on the Kalman filter (KF) to obtain the positioning results. It should be noted that the fusion algorithm is not the focus of this paper, it would be fine to use the Unscented Kalman Filter, Particle Filter, or the factor graph (Sun et al., 2021).

For the cases when the vehicle is in severely occluded environments,, this paper constructs a hybrid temporal neural network-based localization error prediction model, which establishes the mapping relationship between the influence factors (outputs of the INS and observations of the single visible satellite) and the positioning error. When GNSS is available, the training samples are obtained by the tightly coupled integration of GNSS and INS, and the hybrid temporal neural network is well-trained. When severe occlusion of GNSS signal occurs, the acceleration, angular velocity, velocity, and the optional observation of 1 visible satellite (satellite position, pseudo-range, azimuth, and altitude angle) are used as the inputs of the hybrid temporal neural network to obtain the predicted localization error and thereby achieve the compensation. The related diagram is shown in Figure 2.

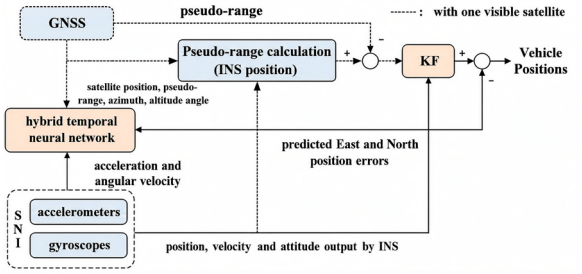

Figure 2. Diagram of the proposed positioning methodology (for the severely occluded environment)

In practice, complex urban environments are randomized to mildly occluded environments (urban canyons) and severely occluded environments (overpasses, tunnels); it is possible to switch between the two strategies depending on the actual number of visible satellites output by the GNSS receiver. Besides, in most cases, the vehicle starts out in an open environment. Thus, the historical satellite position and pseudo-range data needed by the multi-task learning model can be stored by utilizing time windows.

4. GNSS Observation Accuracy Enhancement Based On Multi-task Learning

Figure 3 shows the framework of the multi-task learning model for GNSS observation enhancement. Based on the received historical satellite position data, the satellite position prediction subnetwork is established by the Time Series Forecasting (TSP) method. Then, the satellite pseudo-range prediction subnetwork is designed. Considering that satellite position is one of the key influences on satellite pseudo-range, the high-dimensional features of satellite positions are also introduced into the satellite pseudo-range prediction subnetwork. The

two subnetworks are optimized together by using multi-task learning. Finally, the obtained satellite position and pseudo-range are used for the fusion localization based on KF.

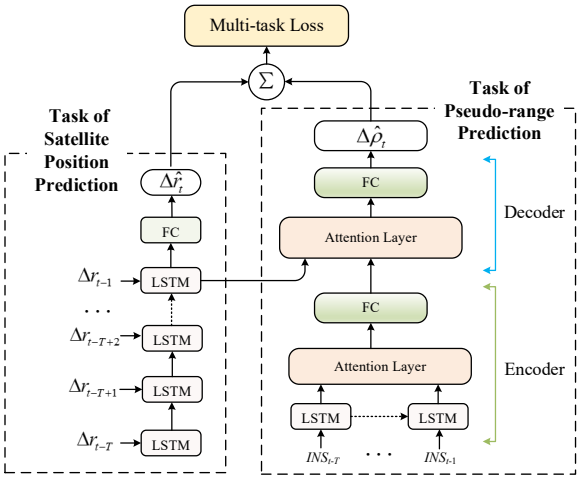

Figure 3. The framework of the multi-task learning-based model for GNSS observation enhancement

4.1 Design of Satellite Position Prediction Subnetwork

The input of the satellite position prediction subtask is $\mathcal{R}_{1:T} = \{\Delta r_1, \Delta r_2, \ldots, \Delta r_T \mid \Delta r_i \in \mathbb{R}^{d_r}\}$, while the output is $\mathcal{R}_{T+1:\tau} = \{\Delta r_{T+1}, \Delta r_{T+2}, \ldots, \Delta r_\tau \mid \Delta r_i \in \mathbb{R}^{d_r}\}$, where Δr_i represents satellite position difference at the moment i, i.e. $\Delta r_i = r_i - r_{i-1}$, T is the window size of the historical satellite position, and τ represents the window size of the satellite predicted position (when τ is 1, it is a single step prediction).

It is difficult for RNNs to learn features with long intervals due to due to gradient disappearance and gradient explosion. LSTM is usually used for time series prediction. Compared with the RNN that only transmits the states forward, LSTM accumulates information over a long timespan through gating and reaches a convergence state.

As shown in Figure 3 the sub-task of satellite position prediction is composed of one layer of LSTM and followed by a fully connected layer to obtain the satellite position difference at the current moment $\Delta\hat{r}_t$. Then, the predicted satellite position can be calculated:

$$\hat{r}^m_{GNSS,S+1} = \hat{r}^m_{GNSS,0} + \sum_{t=1}^{S} \Delta\hat{r}_{GNSS,t} \tag{1}$$

where $\hat{r}^m_{GNSS,0}$ represents the initial satellite position, $\Delta\hat{r}_{GNSS,t}$ is the predicted satellite position difference between adjacent moments, and S is the timespan when the vehicle is in a mildly occluded environment, i.e. the total duration of the satellite position prediction.

4.2 Design of Satellite Pseudo-range Prediction Subnetwork

In the satellite pseudo-range prediction sub-task, the difference between the pseudo-range of the current moment and that of the last moment is predicted, which can be expressed as:

$$\begin{aligned}\Delta\rho^m_{GNSS,i} &= \rho^m_{GNSS,i} - \rho^m_{GNSS,i-1} \\ &= \sqrt{\left(x_i - x_i^m\right)^2 + \left(y_i - y_i^m\right)^2 + \left(z_i - z_i^m\right)^2} - \\ &\sqrt{\left(x_{i-1} - x_{i-1}^m\right)^2 + \left(y_{i-1} - y_{i-1}^m\right)^2 + \left(z_{i-1} - z_{i-1}^m\right)^2} \\ &+ \delta b_{r,i} - \delta b_{r,i-1} + \varepsilon_\rho^m\end{aligned} \tag{2}$$

where $\left[x^m_{i-1}, y^m_{i-1}, z^m_{i-1}\right]$ and $[x_{i-1}, y_{i-1}, z_{i-1}]$ represent the position of the satellite and the receiver at the last moment, respectively. δb_r is the error due to receiver clock error, and ε_0^m represents other errors.

As shown in Figure 3, the encoder part of the satellite pseudo-range prediction subnetwork includes the input embedding LSTM layer and the Attention Layer. The LSTM layer encodes the 3-dimensional accelerations and 3-dimensional angular velocities of the previous T moments to obtain the hidden state. The inputs of the satellite pseudo-range prediction subnetwork are measured by the INS, denoted as INS_t. The number of hidden units of the LSTM layer is 128.

The structure of the decoder part is similar to that of the Attention Layer of the encoder part. Considering that $\Delta\rho$ is affected by both the vehicle motion and the satellite motion, the input of the decoder part includes the output of the encoder and the LSTM hidden layer output of the satellite position prediction task. The output of the encoder contains the vehicle motion features, while the LSTM hidden layer contains the satellite motion features. Finally, the output for the satellite pseudo-range difference at the current moment is obtained. The satellite pseudo-range prediction subtask can be expressed as:

$$\Delta\hat{\rho}^m_{GNSS,t} = f_\theta(INS_{t-T}, \ldots, INS_{t-1}; H_r) \tag{3}$$

where INS_{t-1}, …, INS_{t-T} represents the input sequence of the satellite pseudo-range prediction sub-task, H_r represents the LSTM hidden layer output of the satellite position prediction sub-task and θ is the parameter to be optimized.

The satellite pseudo-range at the current moment can be obtained according to the predicted pseudo-

range difference at the current moment and the initial pseudo-range of the satellite:

$$\hat{\rho}^{m}_{GNSS,S+1} = \rho^{m}_{GNSS,0} + \sum_{t=1}^{S} \Delta\rho_{GNSS,t} \tag{4}$$

where $\hat{\rho}^{m}_{GNSS,0}$ represents the initial satellite pseudo-range, $\Delta\hat{\rho}_{GNSS,t}$ is the predicted pseudo-range difference between time t and the previous moment, and S represents the timespan when the vehicle is in the occluded environment.

Finally, the predicted satellite position and pseudo-range will be used in the measurement update to obtain the position information.

4.3 Strategy of Multi-task Learning

In this paper, the LSTM output of the satellite position prediction subnetwork is used as the input of the decoder of the satellite pseudo-range prediction subnetwork, and the multi-task learning is carried out by balancing the losses between the subtasks. Since the loss of multi-task learning combines the loss of each subtask, balancing the loss of each subtask is the key for optimizing each subtask model (Yao et al., 2017).

The loss weight adjustment method based on training speed conducts the optimization by increasing the loss weight of the subtask with a slow training speed. Based on Zhang et al. (2020), the subtask loss weights of the current iteration are set according to the subtask loss weights of the last iteration:

$$\lambda_i(t) = \frac{C\exp\left(w_i(t-1)/U\right)}{\sum_j \exp\left(w_j(t-1)/U\right)} \tag{5}$$

where $\lambda_i(t)$ is the loss weight of the i-th subtask during the t-th iteration, U is the hyperparameter used for controlling the flexibility of the subtask weight, C is the number of the subtasks, and $w_i(t-1)$ can be expressed as:

$$w_i(t-1) = \frac{L_i(t-1)}{L_i(t-2)} \tag{6}$$

where $L_i(t)$ is the average of the loss of the i-th subtask during the t-th iteration.

In this method, the training speed of each subtask at the current iteration is accurately estimated by the ratio of the training loss for the two previous iterations, and the loss weight is normalized.

The multi-task learning-based model for GNSS observation enhancement includes two kinds of losses: the loss of the satellite position prediction subtask and the loss of the satellite pseudo-range prediction subtask. The loss of the satellite position prediction subtask is defined as:

$$L_r = \frac{1}{N}\frac{1}{S}\sum_{i=1}^{N}\sum_{t=1}^{S}\left\|\Delta\hat{r}_t^i - \Delta\, r_t^i\right\| \tag{7}$$

where $\Delta\hat{r}_t^i$ and Δr_t^i are the predicted satellite position difference and true satellite position difference, respectively. S and N are the sequence length and batch size respectively.

Similarly, the loss of the satellite pseudo-range prediction subtask is expressed as:

$$L_\rho = \frac{1}{N}\frac{1}{S}\sum_{i=1}^{N}\sum_{t=1}^{S}\left\|\Delta\hat{\rho}_t^i - \Delta\rho_t^i\right\| \tag{8}$$

where $\Delta\hat{\rho}_t^i$ and $\Delta\rho_t^i$ are the predicted pseudo-range difference and the true pseudo-range difference, respectively.

Thus, the total loss can be expressed as:

$$L = \lambda_r L_r + \lambda_\rho L_\rho \tag{9}$$

where λ_r and λ_ρ are the loss weight coefficients of the satellite position prediction subtask and of the satellite pseudo-range prediction subtask, respectively. They are dynamically adjusted according to the loss during the training process.

5. Localization Error Prediction Model Based on Hybrid Temporal Neural Network

The framework of the localization error prediction model based on the hybrid temporal neural network is depicted in Figure 4. The hybrid temporal neural network includes two models, i.e. the LSTM pre-training model and the observation fusion model.

If there is no visible satellite, the LSTM pre-training model takes the INS output of the previous T moments as the input to get the predicted value of the INS error. In other words, the predicted localization error is only provided by the LSTM pre-training model when there is no visible satellite.

If there is 1 visible satellite, the predicted localization error is provided by the observation fusion model. However, both the INS outputs and the satellite observations received by GNSS at the current moment are used as the inputs of the hybrid temporal neural network. The LSTM pre-training model is also used for providing the features of

the INS outputs, which are concatenated in the observation fusion model. The positioning error is compensated on the basis of tightly coupled fusion positioning using the 1 visible satellite.

In this paper, the positioning error is divided into east position error and north position error. When GNSS is available, the fusion positioning based on KF can achieve a high accuracy. In this case, the true value of the positioning error can be obtained by simulating satellite failure.

When simulating a scenario with no visible satellite, the truth value of the LSTM pre-training model can be obtained, i.e. the positioning error of INS, which is the difference between the positioning results output by INS and the fusion positioning results. When simulating a scenario in which the GNSS can receive the observations of only 1 satellite, the truth value of the hybrid temporal neural network can be obtained, i.e. the difference between the tightly coupled integration using 1 satellite and the tightly coupled integration using all visible satellites.

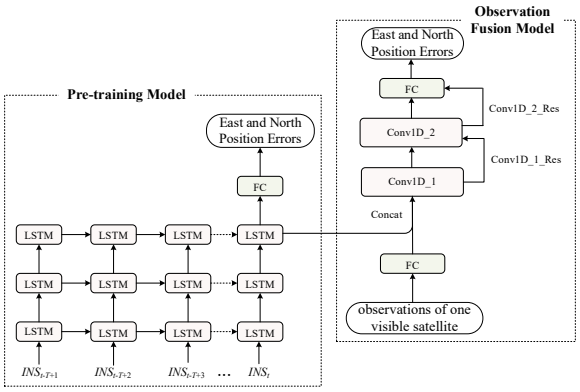

Figure 4. The framework of the proposed localization error prediction model

The localization error prediction model based on the hybrid temporal neural network is the observation fusion model, which mainly includes a one-dimensional convolution. A two-dimensional convolutional layer is usually used for extracting image features, and a one-dimensional convolutional layer is usually used for extracting sequence features (Zhang et al., 2021). Therefore, the features of the LSTM hidden layer and the observations of one satellite are extracted through one-dimensional convolutional networks. Besides, inspired by the residual connection mentioned in (Zheng et al., 2023), the observation fusion model proposed in this paper mainly consists of two one-dimensional convolutional layers and two one-dimensional residual convolution layers.

Firstly, the observations of one satellite are transformed by a fully connected layer, and then the output is concatenated with the output of the last hidden layer of the LSTM pre-training model to obtain the input features of the observation fusion model:

$$x_{in} = \text{Concat}(H_t, x_{sat}) \tag{10}$$

where $x_{in} \in \mathbb{R}^{N\times 2\times d_h}$ represents the input features of the observation fusion model, N represents the batch size, d_h represents the number of the hidden units of the LSTM pre-training model, Concat(·) represents the concatenation of input features, and $H_t \in \mathbb{R}^{N\times d_h}$ represents the output of the last hidden layer of the LSTM pre-training model. $x_{sat} \in \mathbb{R}^{N\times d_h}$ represents the input features related to the observations of one visible satellite extracted by the fully connected layer and activation function, which can be expressed as：

$$x_{sat} = \text{Relu}(sW_1 + b_1) \tag{11}$$

where Relu is the activation function, $s \in \mathbb{R}^{N\times d_s}$ represents the observations of the satellite, including the three-dimensional position of the satellite, the signal-to-noise ratio, the azimuth angle, the altitude angle, and the satellite pseudo-range, thus d_s is 7. $W_1 \in \mathbb{R}^{d_s\times d_h}$ and $b_1 \in \mathbb{R}^{1\times d_h}$ are the weight and bias of the fully connected layer, respectively.

Then, the features x_{in} obtained after concatenation are used as the input of the one-dimensional convolution:

$$x_c = \text{Relu}(\text{BN}(\text{Conv1D\_1}(x_{in}))) \tag{12}$$

where $x_c \in \mathbb{R}^{N\times 2\times 64}$ represents the output of the one-dimensional convolutional layer.

As it is different from the ordinary one-dimensional convolutional layer, the residual convolution layer does not have a batch normalization layer or an activation function layer, and the features are extracted by residual convolution, which can be expressed as:

$$x_{cr} = \text{Conv1D\_1\_Res}(x_{in}) \tag{13}$$

where $x_{cr} \in \mathbb{R}^{N\text{x}2\text{x}64}$ is the output of the residual convolution.

Finally, the output of the current layer $x_{co1} \in \mathbb{R}^{N\text{x}2\text{x}64}$ is obtained by concatenating the output of the one-dimensional convolution and residual convolution:

$$x_{co1} = \text{Concat}(x_c, x_{cr}) \tag{14}$$

Similarly, the calculation of the second one-dimensional convolution layer and residual convolution layer can be expressed as:

$$x_{co2} = \text{Concat}(\text{Relu}(\text{BN}(\text{Conv1D\_2}(x_{co1}))), \text{Conv1D\_2\_Res}(x_{co1})) \quad (15)$$

where $x_{co2} \in \mathbb{R}^{N\times 8\times 32}$ denotes feature output by the second convolutional layer.

Then, x_{co2} is expanded and transformed by a fully connected layer. Finally, the east and north position errors under tight coupling conditions with one satellite are obtained:

$$\delta\hat{p}(t) = \text{Reshape}(x_{co2})W_2 + b_2 \quad (16)$$

where $\delta\hat{p}(t) \in \mathbb{R}^{1\times 2}$ denote the east and north position errors output by the hybrid temporal neural network at the current moment, Reshape means expanding the output of the second one-dimensional convolution layer x_{co2} into a one-dimensional vector, and $W_2 \in \mathbb{R}^{256\times 2}$ and $b_2 \in \mathbb{R}^{1\times 2}$ are the weights and biases of the fully connected layer, respectively.

Based on the hidden layer data of the LSTM pre-training model and the satellite observations, the east and north position errors obtained by the hybrid temporal neural network can be expressed as:

$$\delta\hat{p}(t) = f(s(t); H_t) \quad (17)$$

where f represents the one-dimensional convolution-based observation fusion model, and *s(t)* represents the observations of the 1 visible satellite received at the current moment, including satellite position, pseudo-range, azimuth, and altitude angle. H_t is the output of the last hidden layer of the LSTM pre-training model.

In the hybrid temporal neural network, the LSTM pre-training model acts as the encoder of INS observations, and the one-dimensional convolution-based observation fusion model makes full use of the observations of one visible satellite to correct the position error predicted by the LSTM pre-training model.

The position error compensation of the hybrid temporal neural network is similar to the LSTM pre-training model and it can be expressed as:

$$\hat{p}(t) = p_{1sat}(t) + \delta\hat{p}(t) \quad (18)$$

where $\delta\hat{p}(t) \in \mathbb{R}^{1\times 2}$ and $\hat{p}(t) \in \mathbb{R}^{1\times 2}$ represent the position error compensation information output by the hybrid temporal neural network and the position after compensation, respectively. $p_{1sat}(t) \in \mathbb{R}^{1\times 2}$ is the position obtained by tight coupling using the observation of one satellite.

Similarly to the LSTM pre-training model, the loss function of the hybrid temporal neural network uses the MSE loss function.

6. Experimental Validation

The performance of the proposed positioning methodology is examined based on several road-test experiments carried out in Nanjing. The duration of the selected training and validation datasets is 4680s and 2160s, respectively. For the testing trajectory, six simulated 90 seconds GNSS occluded zones were intentionally introduced at different locations. Different dynamics and motion types (straight, curve, and 90 degrees turn) were considered when choosing the simulated GNSS occluded zone. Moreover, an accurate and reliable NovAtel SPAN-CPT system was used as a reference for quantitative comparison purposes. The horizontal position accuracy of the SPAN-CPT system was 0.01 m without GPS outages.

It should be mentioned here that the position errors further on denote the horizontal Euclidean distance errors between the estimated position and the corresponding reference, which is the main concern for land vehicles.

All the experiments presented in this paper were conducted on a computer equipped with an NVIDIA GeForce GTX 2080Ti GPU, an Intel Core i7-7820X CPU @ 3.6 GHz, and 64 GB of RAM. The average time for one calculation of the GNSS observation enhancement model based on multi-task learning is 0.37ms, while it takes 0.12ms to complete one calculation of the localization error prediction model based on the hybrid temporal neural network.

6.1 Performance Evaluation for the Mildly Occluded Environment

6.1.1 Localization Results with 3 Visible Satellites

In order to verify the effectiveness of the enhanced positioning method based on multi-task learning proposed in this paper, observations prediction for one satellite and two satellite observations were tested by simulation. That is, when the number of visible satellites was 2 or 3 in mildly occluded environments, the GNSS observations can be

supplemented to 4 satellites after observation enhancement, and then the KF algorithm is executed to obtain the fusion positioning results.

Table 1 shows the RMS and maximum errors of the two positioning methods with the predicted observations of one satellite for the six selected testing intervals. The GNSS Observation Enhancement method uses the observations of three visible satellites and the predicted observations of one satellite, while the tightly coupled GNSS/INS integrated positioning method only uses the observations of three visible satellites. The GNSS Observation Enhancement method obtains an average RMS of 1.84m among the six testing intervals, compared with the average RMS of 4.65m obtained by the Tight Coupling method, the error decreases by 60.4%. Besides, the maximum positioning error of the GNSS Observation Enhancement method is 61.6% lower than that of the Tight Coupling method.

Figure 5 shows the positioning errors of the two methods for the straight line of interval 1. The RMS error of the proposed GNSS Observation Enhancement method is 1.42m, which is 63.7% lower than that of the Tight Coupling Method. The maximum positioning error of the proposed GNSS Observation Enhancement method is 3.82 m, which represents a decrease of 66.3% compared with the Tight Coupling Method, which obtained a maximum positioning error of 11.32 m.

Since both the satellite position prediction and pseudo-range prediction tasks are cumulative processes, the prediction errors accumulate with the prediction time. Thus, the positioning errors of the GNSS Observation Enhancement method after KF fusion are also positively correlated with the prediction time. However, the errors of the GNSS Observation Enhancement method are overall smaller in comparison with those of the Tight Coupling Method with 3 visible satellites.

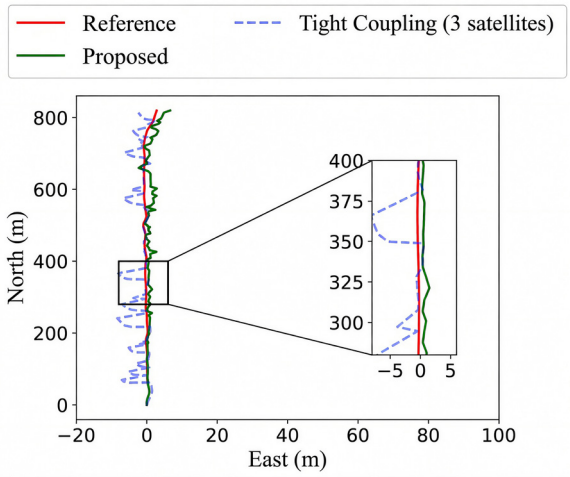

Figure 5. Positioning results with 3 visible satellites during interval 1

6.1.2 Localization Results with 2 Visible Satellites

In order to further verify the effectiveness of the proposed positioning method using the multi-task learning-based model for GNSS observation enhancement, the positioning results for using the predicted observations of 2 satellites are also evaluated. Table 2 shows the RMS and maximum error statistics of the two positioning results during the same six testing intervals.

Table 1. Positioning Errors for 3 Visible Satellites (unit: m)

Interval	Proposed GNSS Observation Enhancement Method		Tight Coupling Method (3 visible satellites)	
	RMS	Maximum	RMS	Maximum
1	1.42	3.82	3.91	11.32
2	1.95	5.84	5.11	13.74
3	1.76	4.96	4.38	12.78
4	2.28	5.07	5.23	15.90
5	1.74	4.67	4.29	12.93
6	1.92	5.21	4.98	13.81

Table 2. Positioning Errors for 2 Visible Satellites (unit: m)

Interval	Proposed GNSS Observation Enhancement Method		Tight Coupling Method (2 visible satellites)	
	RMS	Maximum	RMS	Maximum
1	2.08	5.16	10.23	19.82
2	2.79	7.19	10.69	23.65
3	2.62	6.17	9.82	21.68
4	2.85	6.33	8.48	27.78
5	2.57	6.78	8.76	20.28
6	2.72	6.31	9.39	21.91

Similarly, the GNSS Observation Enhancement method uses the observations of two visible satellites and the predicted observations of two other satellites, and the Tightly coupled GNSS/INS integrated positioning method obtains the positioning results directly from the two visible satellites.

The average RMS error of the GNSS Observation Enhancement method among all the six testing intervals is 2.61 m, while the average RMS error of the Tight Coupling Method is 9.56 m. Thus, the accuracy of the GNSS Observation Enhancement method is improved by 72.7% compared with the Tight Coupling Method with two visible satellites.

Since more observations are predicted when there are 2 visible satellites, higher prediction errors are introduced in the fusion procedure of KF. Thus, the positioning error is normally higher than in the previous scenario, which involved predicting the observations of 1 satellite. Compared with the previous scenario, the RMS and maximum positioning error are 41.2% and 28.3% higher on average, respectively.

6.2 Performance Evaluation for the Severely Occluded Environment

Before training the hybrid temporal neural network, the LSTM model is pre-trained. The LSTM model is optimized by means of a SGD optimizer, the learning rate is set to 0.003, and the batch size N is set to 8. After training for 200 rounds, the model parameters are saved. When training the hybrid temporal neural network, the parameters of the LSTM pre-training model are loaded, and the observations of one satellite are added by using the one-dimensional convolution for fine-tuning. Adam is chosen as the optimizer. The learning rate is set to 0.001, the weight decay is set to 0.0001. The batch size is also set to 8. When there is no visible satellite, the localization error prediction model uses only the LSTM pre-training model, while when there is 1 visible satellite, the hybrid temporal neural network with both the LSTM pre-training model and the observation fusion model is used.

6.2.1 Positioning Performance Based on the LSTM Pre-training Model (for 0 Visible Satellites)

To verify the performance of the LSTM pre-training model, the deep learning Multilayer Perceptron (MLP) regression model is chosen for comparison purposes. MLP is commonly used for position error prediction in case of GNSS outages. The number of hidden layers of the MLP model is set to 3, and the number of neurons is set to 256, 512, and 256, respectively. The input of the MLP model contains both the input of the LSTM pre-training model and the timestamp. The output and the model optimization parameter values for the MLP model are set to be the same as for the LSTM pre-training model.

Table 3 shows the RMS and maximum error statistics for zero visible satellites during the six testing intervals. The average RMS position error for the six testing intervals after prediction and compensation by the LSTM model is 3.61 m, and after prediction and compensation by the MLP model it is 9.72 m. Meanwhile, the average RMS error generated by the positioning result directly output by the INS is 25.04m. Compared with the MLP-based method and the INS-based method, the positioning accuracy of the proposed LSTM error prediction and compensation method is improved by 62.9% and 86.6%, respectively.

Table 3. Positioning Errors for 0 Visible Satellites (unit: m)

Interval	with LSTM pre-training		with MLP		INS only	
	RMS	Maximum	RMS	Maximum	RMS	Maximum
1	2.93	8.78	7.32	15.29	19.68	50.02
2	3.57	9.95	10.41	19.51	27.58	59.11
3	3.71	10.65	9.73	18.75	21.43	59.36
4	3.52	8.26	9.51	20.31	24.72	64.99
5	3.29	10.24	8.56	16.14	27.96	52.97
6	4.65	11.29	12.76	27.82	28.89	65.79

Figure 6 shows the positioning trajectories and corresponding positioning errors for the three methods for interval 2. Compared with the MLP-based method, the LSTM-based error prediction and compensation method reduced the RMS and maximum error by 65.7% and 49.0%, respectively, while the RMS and maximum error were reduced by 87.0% and 83.2%, respectively, compared with the INS-based method. It can be seen from Figure 6 that the positioning error for all the three methods increases over time, but the positioning error after compensation by the LSTM model is significantly smaller than that obtained by the MLP-based method and the INS-based method.

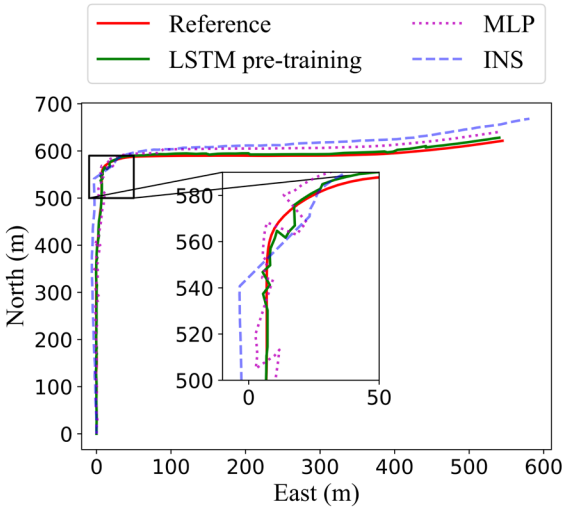

Figure 6. Positioning results with 0 visible satellites during interval 2

6.2.2 Positioning Performance Based on the Hybrid Temporal Neural Network (for 1 Visible Satellite)

Table 4 gives the RMS and maximum error for the positioning results with regard to the error prediction and compensation based on the observations of one visible satellite. The hybrid temporal neural network method uses the INS acceleration, angular velocity, and the observations of one satellite as the input, then the predicted position error is used for compensation to achieve the positioning result. The positioning result for the Tight Coupling Method is based on the KF fusion of the observations for one satellite. The average RMS error for the hybrid temporal neural network method is 3.30m during the six intervals, while for the Tight Coupling Method, it is 21.50m, the aeccuracy of the former being improved by 84.6%. Compared with the LSTM-based method without any satellite observations, the hybrid temporal neural network method achieves an 8.6% improvement.

Figure 7 shows the positioning trajectories and positioning errors during interval 4, respectively, for one visible satellite. The RMS and maximum error of the hybrid temporal neural network method decrease by 82.7% and 83.7%, respectively in comparison with the Tight Coupling Method for 1 visible satellite.

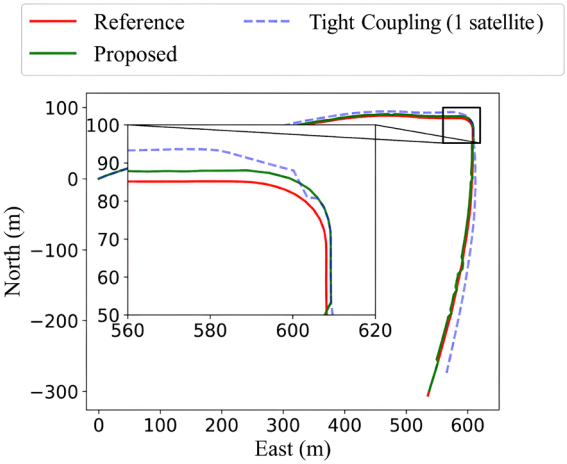

Figure 7. Positioning results with 1 visible satellite during interval 4

Table 4. Positioning Errors for 1 Visible Satellite (unit: m)

Interval	with Proposed Hybrid Temporal Neural Network		Tight Coupling Method (1 visible satellite)	
	RMS	Maximum	RMS	Maximum
1	2.71	8.71	17.29	49.25
2	3.23	8.91	21.01	30.59
3	3.61	9.38	20.54	55.81
4	3.02	7.13	17.48	43.82
5	3.05	8.93	26.69	51.13
6	4.19	10.53	25.97	61.90

7. Conclusion

This paper has presented an intelligent positioning enhancement methodology for land vehicles in two different occluded environments. The goal is to improve the positioning accuracy on the basis of executing the measurement update for visible satellite observations using tightly coupled GNSS/INS.

Two cases are analyzed for each occluded environment in this paper. For the case involving 2 or 3 visible satellites, a multi-task learning model is designed to estimate the satellite position and pseudo-range simultaneously, and thereby supplying additional satellite observations to improve the positioning accuracy. For the case involving 0 satellites or 1 visible satellite, a hybrid temporal neural network with the ability of fitting different INSs and satellite inputs is designed for localization error prediction and compensation.

The proposed methodology has been tested in real road-test experiments. The experimental results indicate that the research fulfills the basic aim of improving the localization accuracy on the basis of making full use of the visible satellites for tightly coupled GNSS/INS.

Future research will consider comparing error prediction performance under different network hyperparameters and exploring other advanced deep learning networks in order to further enhance positioning performance. Furthermore, as vehicle navigation and positioning systems increasingly demand more precise speed and attitude information, future research will also consider methods for the accurate estimation of vehicle speed and attitude.

Acknowledgements

This work was supported in part by the National Key R&D Program of China (Grant No. 2022YFB3904403).

REFERENCES

Adusumilli, S., Bhatt, D., Wang, H. et al. (2015) A novel hybrid approach utilizing principal component regression and random forest regression to bridge the period of GPS outages. *Neurocomputing*. 166, 185-192. https://doi.org/10.1016/j.neucom.2015.03.080.

Ando, T., Kugimiya, W., Hashimoto, T. et al. (2021) Lateral Control in Precision Docking Using RTK-GNSS/INS and LiDAR for Localization. *IEEE Transactions on Intelligent Vehicles*. 6(1), 78-87. https://doi.org/10.1109/TIV.2020.2992857.

Bai, M., Huang, Y., Zhang, Y. et al. (2020) A Novel Progressive Gaussian Approximate Filter for Tightly Coupled GNSS/INS Integration. *IEEE Transactions on Instrumentation and Measurement*. 69(6), 3493-3505. https://doi.org/10.1109/TIM.2019.2932155.

Chu, X., Lu, Z., Gesbert, D. et al. (2021) Vehicle Localization via Cooperative Channel Mapping. *IEEE Transactions on Vehicular Technology*. 70(6), 5719-5733. https://doi.org/10.1109/TVT.2021.3073682.

Fang, W., Jiang, J., Lu. S. et al. (2020) A LSTM Algorithm Estimating Pseudo Measurements for Aiding INS during GNSS Signal Outages. *Remote Sensing*. 12(2), Art. no. 256. https://doi.org/10.3390/rs12020256.

Farag, W. (2021) Real-Time Autonomous Vehicle Localization Based on Particle and Unscented Kalman Filters. *Journal of Control, Automation and Electrical Systems*. 32, 309-325. https://doi.org/10.1007/S40313-020-00666-W.

Gao, L., Xiong, L., Xia, X. et al. (2022) Improved Vehicle Localization Using On-Board Sensors and Vehicle Lateral Velocity. *IEEE Sensors Journal*. 22(7), 6818-6831. https://doi.org/10.1109/JSEN.2022.3150073.

Li, J., Song, N., Yang, G. et al. (2017) Improving positioning accuracy of vehicular navigation system during GPS outages utilizing ensemble learning algorithm. *Information Fusion.* 35(C), 1-10. https://doi.org/10.1016/j.inffus.2016.08.001.

Li, X. & Xu, Q. (2017) A Reliable Fusion Positioning Strategy for Land Vehicles in GPS-Denied Environments Based on Low-Cost Sensors. *IEEE Transactions on Industrial Electronics.* 64(4), 3205-3215. https://doi.org/10.1109/TIE.2016.2637306.

Liu, J. & Guo, G. (2021) Vehicle Localization During GPS Outages With Extended Kalman Filter and Deep Learning. *IEEE Transactions on Instrumentation and Measurement.* 70, Art. no. 7503410. https://doi.org/10.1109/TIM.2021.3097401.

Liu, Q., Gao, C., Shang, R. et al. (2022) NLOS signal detection and correction for smartphone using convolutional neural network and variational mode

decomposition in urban environment. *GPS Solutions.* 27, Art. no. 31. https://doi.org/10.1007/S10291-022-01369-2.

Liu, Y., Luo, Q. & Zhou, Y. (2022) Deep Learning-Enabled Fusion to Bridge GPS Outages for INS/GPS Integrated Navigation. *IEEE Sensors Journal.* 22(9), 8974-8985. https://doi.org/10.1109/JSEN.2022.3155166.

Lu, S., Gong, Y., Luo, H. et al. (2020) Heterogeneous Multi-Task Learning for Multiple Pseudo-Measurement Estimation to Bridge GPS Outages. *IEEE Transactions on Instrumentation and Measurement.* 70, Art. no. 8500916. https://doi.org/10.1109/TIM.2020.3028438.

Murugaiah, P., Samiappan, D. & Nagu, B. (2025) Optimizing Motion in Nanoscale Robotics: A Hybrid WQPSO-Fuzzy Logic Approach for Dynamic Path Planning. *Studies in Informatics and Control.* 34(2), 65-76. https://doi.org/10.24846/v34i2y202506.

Sun, R., Zhang, Z., Cheng, Q. et al. (2021) Pseudorange error prediction for adaptive tightly coupled GNSS/IMU navigation in urban areas. *GPS Solutions*. 26, Art. no. 28. https://doi.org/10.1007/S10291-021-01213-Z

Yao, Y., Xu, X., Zhu, C. et al. (2017) A hybrid fusion algorithm for GPS/INS integration during GPS outages. *Measurement*. 103, 42–51. https://doi.org/10.1016/j.measurement.2017.01.053.

Wang, Y., Liang, M. & Zhao, Y. (2025) Localization and Path Planning for Railway Inspection Robot Based on Multi-Sensor Fusion and Improved ACO. *Studies in Informatics and Control* 34(4), 29-40. https://doi.org/10.24846/v34i4y202503.

Zhang, G., Wen, W., Xu, B. et al. (2020) Extending Shadow Matching to Tightly-Coupled GNSS/INS Integration System. *IEEE Transactions on Vehicular Technology*. 69(5), 4979-4991. https://doi.org/10.1109/TVT.2020.2981093.

Zhang, M., Jia, J., Chen, J. et al. (2021) Indoor Localization Fusing WiFi With Smartphone Inertial Sensors Using LSTM Networks. *IEEE Internet of Things Journal*. 8(17), 13608-13623. https://doi.org/10.1109/JIOT.2021.3067515.

Zheng., Z., Li., X., Zhu., J. et al. (2023) Highly Robust Vehicle Lateral Localization Using Multilevel Robust Network. *IEEE Transactions on Neural Networks and Learning Systems*. 34(7), 3527-3537. https://doi.org/10.1109/TNNLS.2021.3116433.